

Measurement of the μ decay spectrum with the ICARUS liquid Argon TPC

The ICARUS Collaboration

S. Amoruso^a, M. Antonello^b, P. Aprili^c, F. Arneodo^c,
 A. Badertscher^d, B. Baiboussinov^e, M. Baldo Ceolin^e,
 G. Battistoni^f, B. Bekman^g, P. Benetti^h, M. Bischofberger^d,
 A. Borio di Tigliole^h, R. Brunetti^h, R. Bruzzese^a, A. Bueno^{d,i},
 E. Calligarich^h, M. Campanelli^d, F. Carbonara^a,
 C. Carpanese^d, D. Cavalli^f, F. Cavanna^b, P. Cennini^j,
 S. Centro^e, A. Cesana^k, C. Chen^l, D. Chen^l, D.B. Chen^e,
 Y. Chen^l, R. Cidⁱ, K. Cieřlikⁿ, D. Cline^o, A.G. Cocco^a,
 Z. Dai^d, C. De Vecchi^h, A. Dąbrowskaⁿ, A. Di Cicco^a,
 R. Dolfini^h, A. Ereditato^a, M. Felcini^d, A. Ferella^b,
 A. Ferrari^{j,f}, F. Ferri^b, G. Fiorillo^a, S. Galli^b,
 D. Garcia-Gamezⁱ, Y. Ge^d, D. Gibin^e, A. Gigli Berzolari^h,
 I. Gil-Botella^d, K. Graczyk^p, L. Grandi^h, A. Guglielmi^e,
 K. He^l, J. Holeczek^g, X. Huang^l, C. Juszczak^p,
 D. Kielczewska^{q,r}, J. Kisiel^g, T. Kozłowski^r, M. Laffranchi^d,
 J. Lagoda^q, Z. Li^l, F. Lu^l, J. Ma^l, G. Mangano^a,
 G. Mannocchi^{m,1}, M. Markiewiczⁿ, A. Martinez de la Ossaⁱ,
 C. Matthey^o, F. Mauri^h, A. Melgarejoⁱ, A. Menegolli^h,
 G. Meng^e, M. Messina^d, C. Montanari^h, S. Muraro^f,
 S. Navas-Concha^{d,i}, J. Nowak^p, C. Osunaⁱ, S. Otwinowski^o,
 Q. Ouyang^l, O. Palamara^c, D. Pascoli^e, L. Periale^{s,t},
 G.B. Piano Mortari^b, A. Piazzoli^h, P. Picchi^{t,u,s},
 F. Pietropaolo^e, W. Pólchłopek^v, M. Prata^h, T. Rancati^f,
 A. Rappoldi^h, G.L. Raselli^h, J. Rico^d, E. Rondio^r,
 M. Rossella^h, A. Rubbia^d, C. Rubbia^h, P. Sala^{f,d},
 R. Santorelli^a, D. Scannicchio^h, E. Segreto^b, Y. Seo^o,

¹ Also at IFSI del CNR, sezione presso LNF.

F. Sergiampietri^w, J. Sobczyk^p, N. Spinelli^a, J. Stepaniak^r,
R. Sulej^x, M. Szarskaⁿ, M. Szeptycka^r, M. Terrani^k,
R. Velotta^a, S. Ventura^e, C. Vignoli^h, H. Wang^o, X. Wang^a,
J. Woo^o, G. Xu^l, Z. Xu^l, A. Zalewskaⁿ, C. Zhang^l,
Q. Zhang^l, S. Zhen^l, W. Zipper^g

^a*Università Federico II di Napoli e INFN, Napoli, Italy*

^b*Università dell'Aquila e INFN, L'Aquila, Italy*

^c*INFN - Laboratori Nazionali del Gran Sasso, Assergi, Italy*

^d*Institute for Particle Physics, ETH Höngerberg, Zürich, Switzerland*

^e*Università di Padova e INFN, Padova, Italy*

^f*Università di Milano e INFN, Milano, Italy*

^g*Institute of Physics, University of Silesia, Katowice, Poland*

^h*Università di Pavia e INFN, Pavia, Italy*

ⁱ*Dpto de Física Teórica y del Cosmos & C.A.F.P.E., Universidad de Granada, Granada, Spain*

^j*CERN, Geneva, Switzerland*

^k*Politecnico di Milano (CESNEF), Milano, Italy*

^l*IHEP - Academia Sinica, Beijing, People's Republic of China*

^m*Laboratori Nazionali di Frascati (LNF), INFN, Frascati, Italy*

ⁿ*H.Niewodniczański Institute of Nuclear Physics, Kraków, Poland*

^o*Department of Physics, UCLA, Los Angeles, USA*

^p*Institute of Theoretical Physics, Wrocław University, Wrocław, Poland*

^q*Institute of Experimental Physics, Warsaw University, Warszawa, Poland*

^r*A.Soltan Institute for Nuclear Studies, Warszawa, Poland*

^s*IFSI, Torino, Italy*

^t*Università di Torino, Torino, Italy*

^u*INFN Laboratori Nazionali di Frascati, Frascati, Italy*

^v*AGH-University of Science and Technology, Kraków, Poland*

^w*INFN, Pisa, Italy*

^x*Warsaw University of Technology, Warszawa, Poland*

Abstract

Examples are given which prove the ICARUS detector quality through relevant physics measurements. We study the μ decay energy spectrum from a sample of stopping μ events acquired during the test run of the ICARUS T600 detector. This detector allows the spatial reconstruction of the events with fine granularity, hence, the precise measurement of the range and dE/dx of the μ with high sampling rate. This information is used to compute the calibration factors needed for the full calorimetric reconstruction of the events. The Michel ρ parameter is then measured by comparison of the experimental and Monte Carlo simulated μ decay spectra, obtaining $\rho = 0.72 \pm 0.06$ (stat.) ± 0.08 (syst.). The energy resolution for electrons below ~ 50 MeV is finally extracted from the simulated sample, obtaining $(E_{\text{meas}}^e - E_{MC}^e)/E_{MC}^e = 11\%/\sqrt{E}$ [MeV] $\oplus 2\%$.

1 Introduction

The study of muon decay has played in the past a major role for the understanding of weak interactions, being the only accessible purely leptonic process. Muon decay was first described in a model-independent way by Michel [1], using the most general, local, derivative-free, lepton-number conserving, four fermion interaction. For unpolarized muons, the decay probability is given by:

$$\frac{dP}{dx}(x; \rho, \eta) = \frac{1}{N} x^2 \left(3(1-x) + \frac{2}{3} \rho (4x-3) + 3\eta \frac{m_e}{E_{\max}} \frac{1-x}{x} + \frac{1}{2} f(x) + \mathcal{O}\left(\frac{m_e^2}{E_{\max}^2}\right) \right) \quad (1)$$

where N is a normalization factor; $x = \frac{E_e}{E_{\max}}$ is the *reduced* energy (ranging from m_e/E_{\max} to 1); E_e and m_e are respectively the total energy and mass of the electron produced in the decay; $E_{\max} = m_\mu/2$ is the end-point of the spectrum; $f(x)$ is the term accounting for the first order radiative corrections assuming a local V-A interaction [2]; finally, ρ and η are the so-called Michel parameters, defined in terms of bilinear combinations of the coupling constants of the general four fermion interaction, and hence depending on the type of interaction governing the decay process. For the Standard Model (SM) V-A interaction, the parameters take the values $\rho_{\text{SM}} = 0.75$ and $\eta_{\text{SM}} = 0$.

The V-A assumption has already been confirmed in muon decay with high precision [3,4] by the determination of the whole set of Michel parameters and complementary measurements. Figure 1 (left) shows the theoretical shape of the μ decay spectrum for various values of the parameters ρ and η . As shown in the figure, and expected from inspection of Equation 1, the shape of the spectrum is more sensitive to ρ , since η is weighted by $1/x$ and hence determines the shape at low energy. The radiative corrections, shown in Figure 1 (right), determine the shape of the spectrum near the end-point and therefore the value of ρ is very sensitive to them. It has been shown that the overall effect of the radiative corrections on the value of ρ is of the order of 6% [2].

The Michel parameter ρ has been measured in the past by several groups (see Table 1). Peoples [5], Sherwood [6] and Fryberger [7] have measured ρ in the late 60's using the high energy part of the μ decay spectrum assuming the V-A value $\eta = 0$. Derenzo [8] has measured the lower part of the energy spectrum, and combined his data with the previous results (essentially Peoples' measurement) into a common two-parameter fit, to obtain ρ with a precision of about 0.4%, which is the most accurate existing measurement with no assumptions for the value of η . These results have been obtained using dedicated experiments involving data samples of typically several hundreds of thousands of events. More recently, the data from electron-positron colliders have been used to measure the Michel parameters of the purely leptonic τ decay near the Z_0 resonance [9]. These measurements are based on the analysis of samples that typically include several tens of thousands of events.

We present here a further measurement obtained with the ICARUS detector, during its test phase (2001). ICARUS is a project, proposed in 1985 [10], for the installation of a

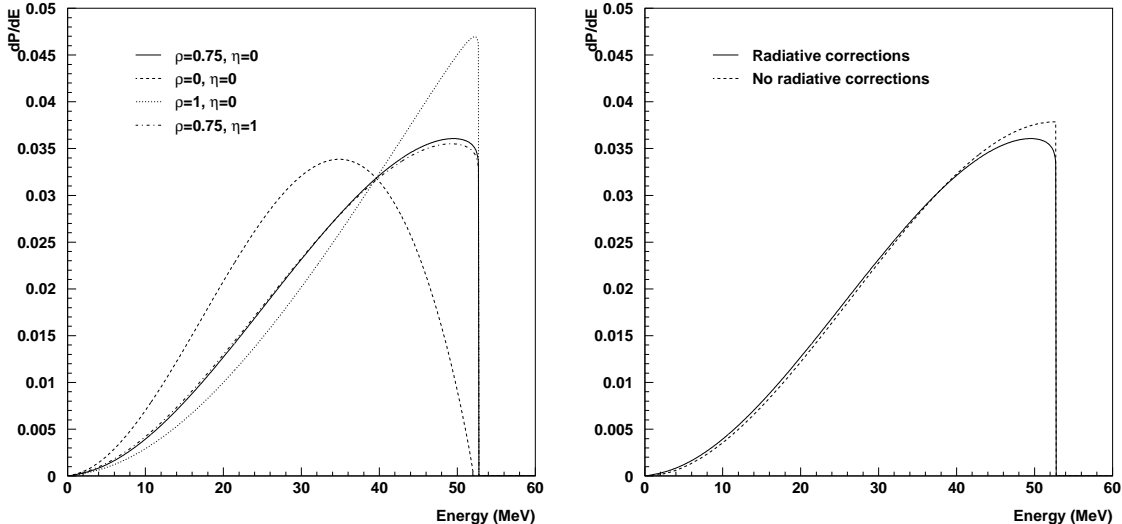


Fig. 1. Left: Muon decay energy spectra for various values of the Michel parameters including the V-A values. Right: Effect of the first order radiative corrections on the muon decay spectrum ($\rho = 0.75$, $\eta = 0$).

large liquid Argon (LAr) time projection chamber (TPC) in the Gran Sasso Laboratory, Italy, for the study of neutrino physics and matter stability [11]. The physics potential of this type of detector has been extensively described elsewhere, both for the final project [10] and its initial phase with the ~ 600 t LAr prototype (ICARUS T600) [12].

The sample of events in which a muon enters, stops and eventually decays in the detector’s sensitive volume –hereafter called *stopping muon* sample– constitutes an important benchmark to evaluate the physics performance of ICARUS. Because of their simple topology, stopping muon events are relatively easy to reconstruct in space, allowing the computation of the different calibration factors needed in the full calorimetric reconstruction. Thus, we can study the muon decay spectrum and measure the Michel ρ parameter, which constitutes the first physics measurement performed with the novel ICARUS detector technology, and proves that the technique is mature enough to produce physics results. Our new result is not competitive with those obtained from μ decay, and barely with those obtained from τ decay. However, it must be remarked that this result has been obtained using 1858 muon decay events with a non optimized experiment. Our result stresses the capabilities of the ICARUS technology to produce robust physics results.

2 Experimental setup

ICARUS T600 [13] is a large cryostat divided in two identical, adjacent half-modules of internal dimensions $3.6 \times 3.9 \times 19.9$ m³, each containing more than 300 t of LAr. Each half-module houses an internal detector composed of two TPC’s (referred to as *Left* and *Right* chambers), the field shaping system (race track electrodes), monitors, probes, photomultipliers, and is externally surrounded by a set of thermal insulation layers. Each TPC is

Author	Value	Assumption
Peoples	0.750 ± 0.003	$\eta \equiv 0$
Sherwood	0.760 ± 0.009	$\eta \equiv 0$
Fryberger	0.762 ± 0.008	$\eta \equiv 0$
Derenzo	0.752 ± 0.003	$-0.13 < \eta < 0.07$
SLD	$0.72 \pm 0.09 \pm 0.03$	lepton univ.ers.
CLEO	$0.747 \pm 0.010 \pm 0.006$	lepton univ.ers.
ARGUS	0.731 ± 0.031	lepton univ.ers.
L3	$0.72 \pm 0.04 \pm 0.02$	lepton univ.ers.
OPAL	$0.78 \pm 0.03 \pm 0.02$	lepton univ.ers.
DELPHI	$0.78 \pm 0.02 \pm 0.02$	lepton univ.ers.
ALEPH	0.742 ± 0.016	lepton univ.ers.
This analysis	$0.72 \pm 0.06 \pm 0.08$	$-0.020 < \eta < 0.006$

Table 1

Results from previous measurements of the Michel ρ parameter. First (second) quoted error is of statistical (systematical) origin. Single error bounds correspond to statistical and systematic errors added in quadrature.

formed by three parallel planes of wires, 3 mm apart, oriented at $0, \pm 60^\circ$ to the horizontal, with 3 mm pitch wires, positioned along the left and right side walls of the half-module. The cathode plane is parallel and equidistant to the wire planes of each TPC. A high voltage system produces a uniform electric field (500 V/cm) perpendicular to the wire planes, forcing the drift of the ionization electrons (the maximal drift path is 1.5 m). The electric field is uniform in the volume contained between the wire planes, the cathode and the planes of race track electrodes (hereafter referred to as LAr *active* volume).

The ionization electrons produced in the LAr active volume drift perpendicularly to the wire planes due to the applied electric field, inducing a signal (*hit*) on the wires near which they are drifting while approaching the different wire planes. By appropriate biasing, the first set of planes can be made non-destructive (*Induction* planes), so that the charge is finally collected in the last plane (*Collection* plane). Each wire plane provides a two-dimensional projection (*view*) of the event, where the position in one coordinate is constrained by the hit wire, while the signal timing with respect to the trigger gives the position along the drift direction. Each track is sampled by a large number of wires. This is one of the main feature of the ICARUS technology, exploited in the present analysis.

A full test of the T600 experimental set-up on the surface of the earth was carried out in Pavia (Italy) during the period April-August 2001. One T600 half-module was fully instrumented to allow a complete test under real experimental conditions. Although the test was mainly intended as a technical run, a substantial amount of cosmic ray data was acquired, since the detector was not shielded against cosmic rays as will be the case in the Gran Sasso underground laboratory. The detector's conditions during data acquisition

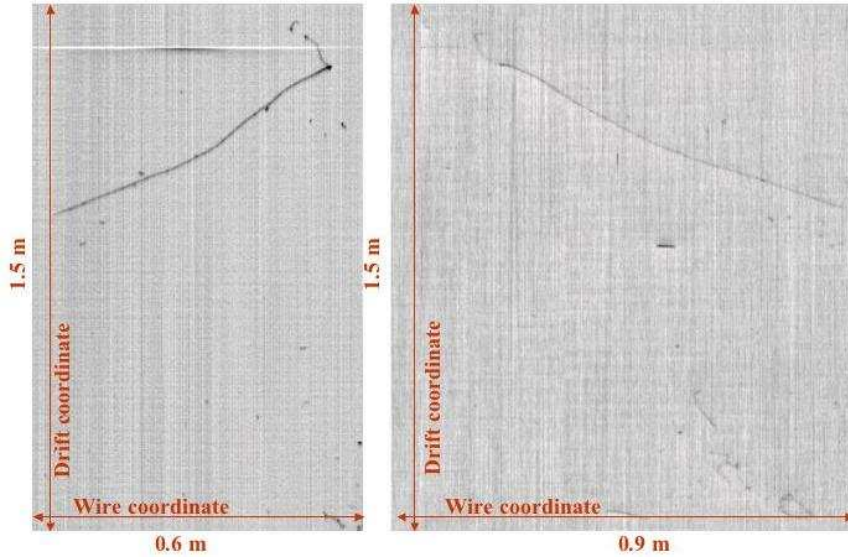


Fig. 2. Run 966 Event 8 Right chamber: muon decay event views corresponding to the Collection (left) and second Induction (right) wire planes.

(DAQ) were not stable, being subject to the optimization of various working parameters of the detector.

One of the main goals of the test run was the detection of long muon tracks crossing the detector at large zenith angles (horizontal muons), extremely useful for an overall test of the detector performance. Therefore, an external trigger system was set up to select the horizontal muon events out of the overwhelming background of atmospheric showers. The system consisted of two plastic scintillator layers suitably positioned and arranged in a proper coincidence trigger logic. In spite of the optimization of the trigger for the acquisition of horizontal muon tracks, other kind of events (in particular, stopping muon events) are expected to be acquired within the DAQ time window. Most of these events can not be directly correlated to the triggering event, hereafter they will be referred to as *out-of-time* events (conversely, those which are correlated to the triggering event will be referred to as *in-time* events).

3 Data selection

Data selection was carried out by visual scanning using topological criteria. Stopping muons can be recognized as minimum ionizing tracks entering the detector, with increasing energy deposition and multiple scattering angle when approaching the stopping point. Two different topologies are expected depending on the process undergone by the stopped muon, namely: decay or nuclear absorption. The probability of the absorption processes has been evaluated to be 73% (0%) for negative (positive) muons [14]. For absorption events ($\mu^- + Ar \rightarrow Cl^* + \nu_\mu$), the excited Cl nucleus decays emitting photons which then may interact via Compton scattering. For decay events, a minimum ionizing electron track

(length shorter² than ~ 23 cm) follows the muon. In the present analysis, both decay and absorption events have been used in the determination of the calibration factors for the calorimetric reconstruction (see section 4.2). Figure 2 shows the two-dimensional projections (produced by the Collection and the second Induction planes respectively) of a typical muon decay event.

In the case of decay events, the muon and electron tracks are separated by the muon stopping point, which is taken as the hit with the maximal ionization. The stopping point is assigned to the muon track. This may produce, for events where the muon and electron tracks partially overlap, a loss of the first hits from the electron track. This effect has been evaluated and introduced in the analysis using a sample of simulated events, as explained in section 5.1.

A total of 5830 triggers were scanned, containing 4548 stopping muon events. Out of them, 3370 (74%) were further selected by the preliminary quality cuts. Among the 1178 rejections, 45% of the cases were events with deficiently measured drift charge since the event happened in a region of the detector where the wires had an inadequate polarization during the run; 25% of the cases were due to an event occurring in a region with a substantial component of high amplitude, correlated noise, which may fake the presence of an ionizing track, hence, distorting the real event; the remaining 30% of rejections were due to several other effects, mainly events not fully contained in the LAr sensitive volume³, failures of the reconstruction program due to complicated topologies or absence of one or more views due to problems of the DAQ system.

4 Data reconstruction

4.1 Spatial reconstruction

A full 3D reconstruction of the selected muon events is first performed. The spatial reconstruction of the muon tracks is needed in order to compute the calibration factors entering the calorimetric reconstruction of the events, as explained in section 4.2.

A detailed description of the spatial reconstruction tools has been reported elsewhere [13,15]. The 3D reconstruction is performed in a hit basis using a three-step procedure:

- (1) First, hits are searched for independently in every wire of each wire plane. Hits are

² The minimum observable track length is given by the wire pitch: 3 mm.

³ An event is considered not to be fully contained if the muon or electron end points (identified by the raise in the energy deposition per unit length) are not present. No further fiducial cut on the LAr sensitive volume is required.

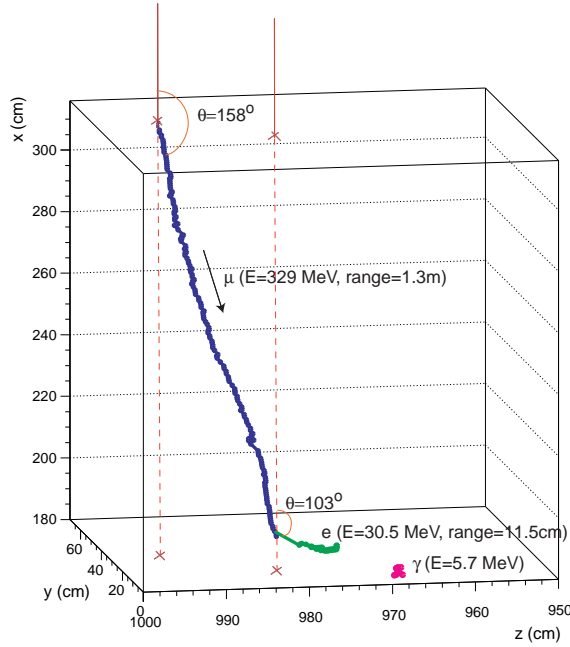


Fig. 3. Run 966 Event 8 Right chamber: fully reconstructed muon decay event.

identified as signal regions of a certain width with output values above the local mean. No information from adjacent wires is used at this stage. A precise determination of the hit position and charge are carried out by means of a fit using an analytical function.

- (2) The identified hits are associated in the second step into 2-dimensional clusters of hits belonging to a common charge deposition, such as tracks or showers. Clusters provide criteria for the identification of the different patterns and for the discrimination between signal and noise hits, based on the cluster hit multiplicity.
- (3) In the third step, the 3D coordinates of the hits from the different reconstructed clusters are computed. Each wire plane constrains two spatial degrees of freedom of the hits, one common to all the wire planes (the drift coordinate) and one specific for each plane (the wire coordinate). The redundancy on the drift coordinate allows the association of hits from different views to a common energy deposition, and together with the wire coordinates from at least two planes, the determination of the hit spatial coordinates.

Figure 3 shows a 3D reconstructed stopping muon event. The muon decay topology is visible, with three reconstructed tracks corresponding to the muon, the decay electron and a $\gamma - e$ conversion, respectively.

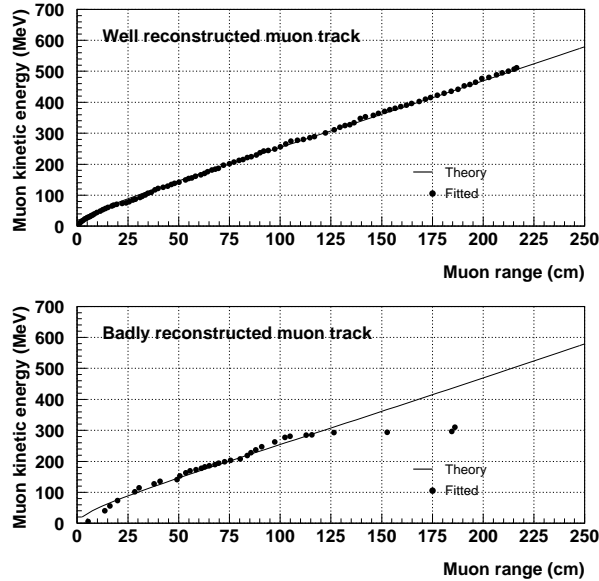


Fig. 4. Kinetic energy vs. range for typical well (top) and badly (bottom) reconstructed muon tracks.

4.2 Calorimetric reconstruction

The ionization charge is precisely measured at the Collection wire plane. The energy associated to a given hit is related to the collected charge by means of

$$E = \frac{CW}{R} e^{(t-t_0)/\tau_e} Q \quad (2)$$

where $C = (152 \pm 2) \times 10^{-4} \text{ fC}/(\text{ADC} \times \mu\text{s})$ is the calibration factor [16]; $W = 23.6_{-0.3}^{+0.5} \text{ eV}$ is the average energy needed for the creation of an electron-ion pair [17]; R is the electron-ion recombination factor; $(t - t_0)$ is the drift time of the electrons; τ_e is the drift electron lifetime, which parametrizes the attachment of drift electrons to impurities in LAR; and Q is the measured charge. R , t_0 and τ_e are extracted from the reconstructed muon tracks, essentially by tuning them so that the measured energy corresponds to the theoretical expectation for stopping muons. This method determines the electron energy in a bias-free way, since all the calibration parameters are tuned using exclusively muon tracks. For the real experimental conditions t_0 is given by the triggering system, but is unknown for most of the stopping muon events used in this analysis, since they are out-of-time events.

Only those tracks successfully reconstructed in space are used in the determination of τ_e and R . A quantitative measurement of the quality of the spatial reconstruction is provided by the goodness of the fit of the muon track to the theoretical kinetic energy vs. range curve, when R , t_0 and τ_e are left as free parameters. A total of 2690 stopping muon events are selected using this method. Two examples of the energy vs. range curve measured for typical well and badly reconstructed muon tracks are shown in Figure 4.

The drift electron lifetime, τ_e , is measured for data taking intervals of 24 hours. The measurement method is based on the observation of the charge attenuation with the drift distance, and has been published elsewhere [16]. However, two main differences must be stressed [15]. First, the charge of a hit depends on the particle momentum, but also on the angle between the track and the wire. Therefore, in general the hit charges are not directly comparable. In order to solve this problem, we normalize each charge with the theoretically expected energy, computed with the Bethe-Bloch formula given the range and length associated to the hit. Second, t_0 is unknown for most of the events, and hence also the absolute drift time/distance. In order to merge hits from different tracks with different t_0 into a common measurement of τ_e , we use the *relative* charge attenuation (rather than *absolute*) as a function of the drift time/distance. Using this method, we obtain values of τ_e ranging from 1.20 to 1.70 ms (depending on the data taking period), in agreement with the results previously published [16]. Data are also compatible with a slight dependence of the electron lifetime on the height: the electron lifetime is about 15% lower at the top than at the bottom of the liquid argon volume, with an almost linear dependence on height. The measured charge is corrected for the attenuation using the value of τ_e averaged for the LAr volume, therefore this decrease is considered as an uncertainty when computing R and introduces a contribution to the total energy resolution $\left. \frac{\Delta E}{E} \right|_{\tau_e} = 5\%$.

R is computed as a function of the theoretical dE/dx (estimated from the range using the Bethe-Bloch formula), by comparing the measured charge (corrected for the finite drift electron lifetime) with the theoretical expectation for stopping muon tracks [15]. Using a sub-sample of 112 in-time events, for which t_0 is known, we obtain $R_{\text{mip}} = 0.640 \pm 0.013$ for minimum ionizing particles, where the error is dominated by the uncertainties of τ_e and of the length of the track segments used to evaluate dE/dx . R_{mip} is used as a reference to tune the value of t_0 for out-of-time events. The uncertainty of this procedure is estimated by applying it to in-time events: the values of t_0 obtained for these events are Gaussian distributed, with mean $2 \pm 9 \mu\text{s}$ and width $82 \pm 8 \mu\text{s}$. This can be interpreted as a negligible shift on the energy scale ($< 0.3\%$) and an extra contribution to the energy resolution of $\left. \frac{\Delta E}{E} \right|_{t_0} = 7\%$. However, it must be stressed that this contribution is due exclusively to the fact that the analyzed events are out-of-time, therefore it will not be present for the detector's real experimental conditions. The whole muon data sample can be used next to compute R for higher values of dE/dx up to $\sim 5 \text{ MeV/cm}$. A linear dependence of R^{-1} on dE/dx with slope $0.11 \pm 0.01 \text{ cm/MeV}$ is found.

5 Results

5.1 Determination of the Michel ρ parameter

From the selected 2690 stopping muon events, a total of 1858 contain electrons available for the determination of the Michel ρ parameter (while the remaining ones are mainly absorption events). The measured energy does not correspond directly to the μ de-

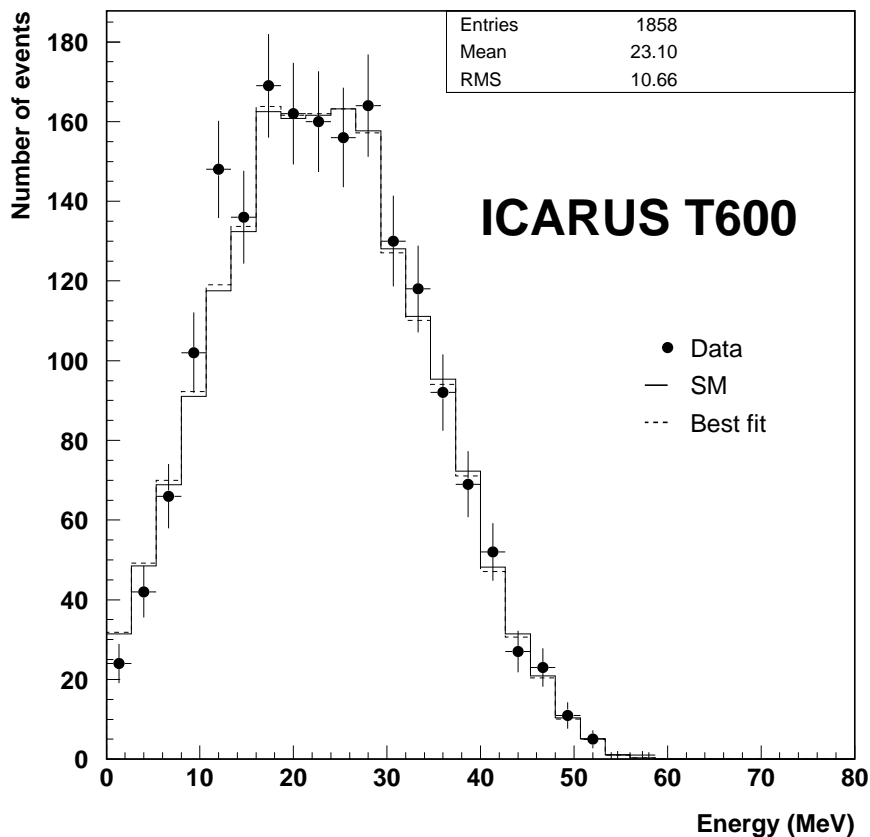


Fig. 5. Energy spectrum of electrons from muon decays in the ICARUS T600 detector (electron energy lost by ionization in LAr). The plot shows the measured distribution (dots) compared both to the SM expectation (solid line) and the best fit with ρ and η as free parameters (dashed line).

cay spectrum (Equation 1) since no attempt to recover the energy loss by Bremsstrahlung radiation has been carried out⁴. The spectrum corresponds to the fraction of the electron energy lost by ionization in LAr. Therefore, in order to measure the Michel ρ parameter we have chosen an approach based on the comparison with a Monte Carlo (MC) simulated event sample. This sample has been generated using FLUKA [18] and consists of 10 000 electrons from muon decay events inside the detector’s sensitive volume. The simulation includes all detector effects except for the presence of impurities in LAr. MC events are reconstructed using the same tools as for the data, and the effect of the impurities and the determination of t_0 are included in average by smearing the measured energy (E) using a Gaussian function of width $\sigma = 0.09E$. The effect of the muon track (which is absent in the MC sample) is the loss of some of the first hits of the electron track due to the overlapping with the muon track. The number of hits of MC electron tracks is found to be on average 2.14 higher than for data electron tracks. Thus, the effect of the muon track can be included on average in the simulation by removing, when computing the energy,

⁴ This does not decrease the statistical accuracy of the measurement and avoids the problem of associating photons to the electron track. Indeed, background conditions in data taking at the surface are such that it was preferred not to worry about a selection of photons pertaining to the electron.

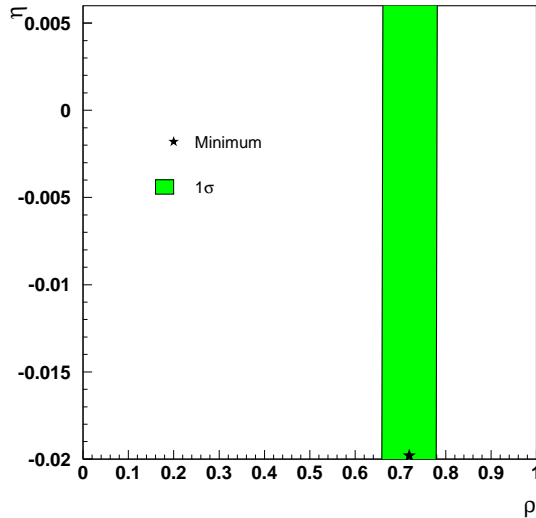


Fig. 6. Results from the fit of the Michel electron spectra. The dot and band show, respectively, the position of the minimum and 1σ region within the considered parameter's space.

the first 2 hits (3 in 14% of the cases) of the electron track. The measured and simulated energy spectra are compared in Figure 5, and they are found to be in good agreement ($\chi^2/ndf = 14.0/20$).

Given the greater sensitivity of the shape of the spectrum to ρ than to η , and the level of correlation between these two parameters (see Equation 1), we measure ρ while constraining η within its experimentally allowed interval ($-0.020 < \eta < 0.006$) [19]. Since the MC sample is generated using the SM values (ρ_{SM} and η_{SM}), the spectrum for an arbitrary pair of values, ρ and η , is built by weighting each MC event with a factor:

$$w = \frac{\frac{dP}{dx}(x_{MC}; \rho, \eta)}{\frac{dP}{dx}(x_{MC}; \rho_{SM}, \eta_{SM})} \quad (3)$$

where $x_{MC} = E_{MC}/E_{max}$, and E_{MC} is the generated energy. We extract the value of ρ as that for which the best fit between the simulated and measured energy spectra is obtained, which yields $\rho = 0.72 \pm 0.06$, where the error has a statistical origin and includes the correlation with η . Figure 6 shows the best fit point and the 1σ region of the fit within the considered Michel ρ - η plane. As expected, our measurement has no sensitivity for the determination of η within the considered experimental bounds, and yields a stable value of ρ for the whole allowed η range.

There are two types of systematic uncertainties that can affect this measurement, namely: a bad estimate of the energy resolution and a systematic shift in the global energy scale. Using the MC sample, the uncertainty of ρ is estimated to be 0.01 (0.03) for an extra $\pm 5\%$ ($\pm 10\%$) contribution to the energy resolution, and 0.04 (0.08) for a shift in the energy scale of $\pm 1\%$ ($\pm 2\%$). The energy resolution is determined essentially by the wire's signal-to-noise (S/N) ratio and the additional contributions from the drift electron lifetime, recombination and t_0 corrections. All these contributions have been extracted from the

data and included in the MC sample, and its uncertainty is estimated to be smaller than 5%. Furthermore, the effect on the final result becomes negligible by removing the last two bins of the electron spectrum when performing the fit. Conversely, the absolute energy scale is given by R , which is determined for minimum ionizing particles with an accuracy of 2% including systematic effects (see section 4.2). Therefore, the total error is dominated at this level by the systematics due to the uncertainty in the energy scale. With a more precise calibration method, which will be available in the real experimental conditions, it is reasonable to think that the absolute energy scale will be known to the 1% level, hence reducing the systematic error of ρ to 0.04. Conversely, with the calibration method used in this analysis, the error of the absolute energy scale is dominated by the systematics on the determination of the length of the muon track segments. Therefore, no further improvement of the result can be foreseen by using a larger data sample. The final result is:

$$\rho = 0.72 \pm 0.06 \text{ (stat.)} \pm 0.08 \text{ (syst.)} \quad (4)$$

which is compatible with the V-A value.

5.2 Energy resolution

The high level of agreement between the experimental and the generated muon decay spectra allows us to estimate the detector's energy resolution using the simulated sample. We have evaluated separately the contributions to the final energy resolution coming from the following sources:

- **Electronic noise:** This contribution depends on the S/N ratio. For non-correlated noise and constant S/N ratio (which is a good approximation of the real experimental conditions) this contribution is expected to vanish at high energies (i.e. for high numbers of wires).
- **Reconstruction effects:** This contribution is intrinsic to the signal extraction method we use, and independent of the energy. The main contribution comes from hits whose shape is not well reproduced by the fitting function. Such a case may arise for tracks with small angle with respect to the drift direction, or unresolved close hits [15]. Other minor contributions are due to undetected hits or fake hits created during the automatic reconstruction procedure.
- **Calorimetric calibration:** As already mentioned in Section 4.2, an extra contribution to the energy resolution is expected when correcting for the electron attachment to impurities using an average value of the drift electron lifetime. This contribution is also energy independent and has been estimated in Section 4.2. In the case of this particular analysis, we have also considered an extra contribution to the energy resolution coming from the determination of t_0 for the different events.

The first two contributions have been evaluated with MC samples generated in the appropriate conditions (see Figure 7). In both cases, the energy resolution is defined as $(E_{\text{meas}}^e - E_{\text{MC}}^e)/E_{\text{MC}}^e$, where E_{MC}^e and E_{meas}^e are, respectively, the MC generated and measured energy of the electron track, disregarding bremsstrahlung losses (i.e. only the

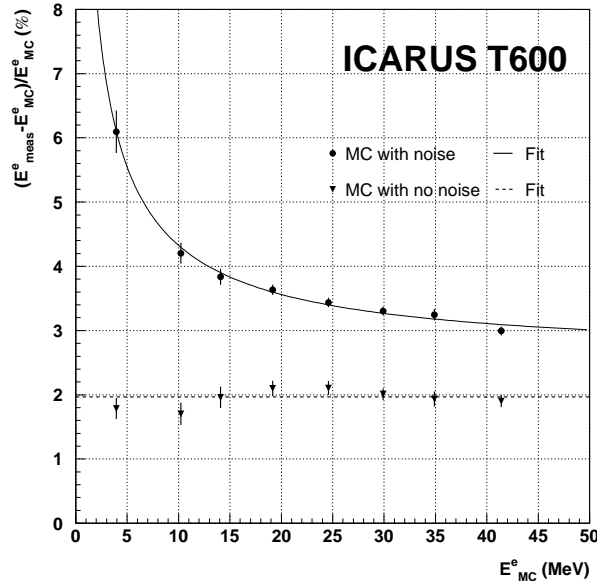


Fig. 7. Energy resolution as a function of the electron energy.

fraction of the energy lost by the electron by ionization of Ar atoms is compared). For every E_{MC}^e bin, the central value and error of the resolution are obtained from a Gaussian fit, with errors of a statistical nature.

In order to evaluate the energy resolution expected from the reconstruction effects, we have generated the MC sample with no electronic noise, and passed it through the whole reconstruction chain. In such a case, we obtain a constant resolution of $(1.97 \pm 0.05)\%$ (see Figure 7). Conversely, the joint effect of the electronic noise and the reconstruction is evaluated with the MC sample generated including the electronic noise. A fit to the points is performed by the function $(E_{meas}^e - E_{MC}^e)/E_{MC}^e = a/\sqrt{E} [\text{MeV}] \oplus b$, where the best fit is obtained for (errors are of statistical origin) $a = (11 \pm 1)\%$ and $b = (2.5 \pm 0.3)\%$ (see Figure 7). This result is compatible with the assumption of a vanishing contribution of the electronic noise at high energies.

6 Conclusions

We have performed the first physics measurement with the ICARUS LAr TPC detection technique: the determination of the Michel ρ parameter from the detailed study of the muon decay spectrum using the stopping muon event sample from the ICARUS T600 detector test run with cosmic rays. We obtain $\rho = 0.72 \pm 0.06$ (stat.) ± 0.08 (syst.), in agreement with the SM value $\rho = 0.75$. This measurement involves the exploitation of both spatial and calorimetric reconstruction capabilities of the detector. Therefore, the obtained result constitutes a proof of the maturity of the detection technique to produce high quality physics results, in view of the operation of the detector in the Gran Sasso

underground laboratory. We have also estimated the energy resolution including detector and reconstruction effects from a sample of MC simulated Michel electrons, obtaining $(E_{\text{meas}}^e - E_{\text{MC}}^e)/E_{\text{MC}}^e$ compatible with $11\%/\sqrt{E} [\text{MeV}] \oplus 2\%$, where the raise at low energies is due to the electronic noise, and the constant term arises from reconstruction effects.

Acknowledgments

We warmly acknowledge N. Makrouchina, F. Varanini and S. Levorato for their contribution to the scanning of the stopping muon events. In addition, we would like to warmly thank the many technical collaborators that contributed to the construction of the T600 detector and to its operation. We are glad of the financial and technical support of our funding agencies and in particular of the Istituto Nazionale di Fisica Nucleare (INFN), of ETH Zürich and of the Fonds National Suisse de la Recherche Scientifique, Switzerland. The Polish groups acknowledge the support of the State Committee for Scientific Research in Poland, 2P03B09520, 2P03B13622, 105,160,620,621/E-344,E-340,E-77,E-78/SPS/ICARUS/P-03/DZ211-214/2003-2005; the INFN, FAI program; the EU Commission, TARI-HPRI-CT-2001-00149. The Spanish group is supported by the Ministry of Science and Technology (project FPA2002-01835).

References

- [1] L. Michel, Proc. Phys. Rep. **A63** (1950) 514.
- [2] R. E. Behrends, R. J. Finkelstein and A. Sirlin, Phys. Rev. **101** (1956) 866.
T. Kinoshita and A. Sirlin, Phys. Rev. **113** (1959) 1652.
- [3] W. Fetscher, H. J. Gerber and K. F. Johnson, Phys. Lett. **B173** (1986) 102.
- [4] Particle Data Group (K. Hagiwara *et al.*), Phys. Rev. **D66** (2002) 010001.
- [5] J. Peoples, Columbia University Report No. NEVIS-147, 1966 (Unpublished).
M. Bardon *et al.*, Phys. Rev. Lett. **14** (1965) 449.
- [6] B. A. Sherwood, Phys. Rev. **156** (1967) 1475.
- [7] D. Fryberger, Phys. Rev. **166** (1968) 1379.
- [8] S. E. Derenzo, Phys. Rev. **181** (1969) 1854.
- [9] SLD Collaboration (K. Abe *et al.*), Phys. Rev. Lett. **78** (1997) 4691.
CLEO Collaboration (J. P. Alexander *et al.*) Phys. Rev. **D56** (1997) 5320.
ARGUS Collaboration (H. Albrecht *et al.*), Phys. Lett. **B431** (1998) 179.
L3 Collaboration (M. Acciarri *et al.*), Phys. Lett. **B438** (1998) 405.
OPAL Collaboration (K. Ackerstaff *et al.*), Eur. Phys. J. **C8** (1999) 3.
DELPHI Collaboration (P. Abreu *et al.*), Eur. Phys. J. **C16** (2000) 229.
ALEPH Collaboration (A. Heister *et al.*), Eur. Phys. J. **C22** (2001) 217.

- [10] ICARUS Collaboration, “ICARUS-I: a proposal for the Gran Sasso Laboratory”, INFN/AE-85/7, Frascati (Italy), 1985. ICARUS Collaboration, “ICARUS-II: A Second-Generation Proton Decay Experiment and Neutrino Observatory at the Gran Sasso Laboratory”, Proposal Vol. I & II, LNGS-94/99, 1994.
- [11] C. Rubbia, “The Liquid Argon Time Projection Chamber: a New Concept for Neutrino Detector”, CERN-EP/77-08, 1977.
- [12] ICARUS Collaboration, “The ICARUS Experiment: A Second-Generation Proton Decay Experiment and Neutrino Observatory at the Gran Sasso Laboratory”, LNGS, P28/01, LNGS-EXP 13/89 add. 1/01, arXiv: hep-ex/0103008.
- [13] ICARUS Collaboration, S. Amoruso *et al.*, *Design, construction and tests of the ICARUS T600 detector*. Preprint submitted to Nucl. Instrum. Meth. **A**.
- [14] H. Primakoff, Rev. Mod. Phys. **31** (1959) 802.
J. C. Sens, Phys. Rev. **113** (1959) 679.
A. Bertin *et al.*, Phys. Rev. **A7**, Comments and Addenda (1973) 2214.
- [15] J. Rico, *First Study of the Stopping Muon Sample with the ICARUS T600 Detector*, Ph.D. Dissertation, ETH 14906, 2002. Available at: <http://neutrino.ethz.ch/diplomathesis.html>.
- [16] ICARUS Collaboration, S. Amoruso *et al.*, *Analysis of the liquid Argon purity in the ICARUS T600 TPC*. Nucl. Instrum. Meth. **A** (article in press).
- [17] M. Miyajima *et al.*, Phys. Rev. **A9** (1974) 1438.
- [18] A. Fassò, A. Ferrari, J. Ranft and P. R. Sala, “Electron-photon transport in FLUKA: status”, Proc. of the Monte Carlo 2000 Conference, Lisbon, 23-26 October 2000, A. Kling *et al.* eds., (Springer, Berlin, 2001).
- [19] H. Burkhard *et al.*, Phys. Lett. **B160** (1985) 343.